

Embedded-atom interatomic potentials for hydrogen in metals and intermetallic alloys

M. Ruda

Centro Atómico Bariloche, 8400 Bariloche, Argentina

D. Farkas

Department of Materials Science and Engineering, Virginia Polytechnic Institute, Blacksburg, Virginia 24061

J. Abriata

Centro Atómico Bariloche, 8400 Bariloche, Argentina

(Received 22 May 1996)

Interatomic potentials of the embedded-atom type have been developed for H in metals. The potentials are constructed through a fitting procedure involving the thermodynamic heat of solution of H in the various metals and the volume expansion of the host lattice upon the dissolution of H. The potentials have been developed in such a way that the same functions for hydrogen are used for all the metals considered and the resulting set of potentials is suitable for the study of hydrogen effects in alloys. The pure metals considered are Ni, Al, Ti, Zr, and Fe. The heats of solution of hydrogen in various intermetallic alloys formed by these metals (TiAl, Ti₃Al, NiAl, Ni₃Al, NiTi, and FeAl) have been studied using the developed potentials in conjunction with existing potentials for the intermetallic systems. The effects of increasing hydrogen absorbed in the host are also simulated for the case of Ni. [S0163-1829(96)06038-9]

I. INTRODUCTION

Interest in understanding the physics of hydrogen in metals and alloys has been continuously increasing for many reasons. On one side there are the practical uses of metal-hydrogen systems such as: storage of hydrogen for clean energy purposes, catalyzers, or absorption of nuclear radiation; on the other, there are unwanted effects on the materials properties caused by small amounts of hydrogen dissolved in metals, such as embrittlement, crack propagation, and corrosion. There is extensive literature dealing with these issues, ranging from first-principles calculations to engineering applications (see for example, Ref. 1).

Atomistic studies of the structures of intermetallic materials have been of great value in the modeling and understanding of alloy behavior. The embedded-atom method (EAM) (Refs. 2 and 3) is normally used for this type of atomistic simulation. The method has been applied in the past to study hydrogen interactions with pure metals, such as Ni and Pd; for a recent review on the subject see Myers and Baskes.⁴ The purpose of the present work was to develop EAM potentials suitable for the study of hydrogen effects in alloys and intermetallic compounds.

The embedded atom formalism calculates the energy of a block of atoms as follows:²

$$E = \sum_{i,j} \frac{1}{2} V(r_{ij}) + \sum_i F(\rho_i), \quad (1)$$

$$\rho_i = \sum_{i,j} \phi(r_{ij}), \quad (2)$$

where E is the total internal energy, V is the pair potential between atoms i and j , F is the embedding function, ρ is the electronic density at atom i due to all other atoms, ϕ is the

electron density at atom i due to atom j as a function of the distance r_{ij} between them. For an alloy model, the pair function, the embedding function, and the electronic density function must be specified for each participating atomic species, and interatomic pair potentials should be obtained for each possible combination of all atomic species. As shown by Johnson,⁵ the electron density functions are determined within a scaling factor to fit monoatomic properties. This is because it is possible to transfer energetic contributions from the pair part to the many-body term or vice versa without affecting the total energy results for any simulation block of a single species. The relative scaling factor between elements should be specified for all the elements that enter an alloy model. One widely used method for specifying the relative pair and many-body contributions for each species is to use the so-called "effective pair approach," where the first derivative of the embedding function calculated for the perfect lattice of each species ρ is set to zero. In addition to this possible transfer of energetic contributions among the pair and many-body terms, the electronic density values can be normalized to any desired value without changing the overall energy for single species simulations provided the embedding functions are modified accordingly. For alloys, the values that are used for the electronic density of the perfect lattice of each species are important and can possibly be used as one more fitting parameter of the alloy model.

The possibility of using H in an alloy in an EAM simulation requires the development of separate H interactions with all components in the alloy. The compatibility requirement is that the same functions for H are used in all cases. We will concentrate on Ni, Al, Ti, Zr, and Fe. The interactions of H with these metals are of great practical interest due to the embrittling effect of H dissolved in the grain boundaries of the intermetallics.

TABLE I. Interatomic potentials used for the various pure metals and alloys.

Materials	References
Ni	Voter and Chen (Ref. 6)
Al	Voter and Chen (Ref. 6)
Ti	Pasianot and Savino (Ref. 9)
Zr	Igarashi <i>et al.</i> (Ref. 8)
Fe	Simonelli <i>et al.</i> (Ref. 11)
Ni-Al	Farkas <i>et al.</i> (Ref. 15)
Ti-Al	Farkas (Ref. 31)
Fe-Al	Vailhé <i>et al.</i> (Ref. 18)
Ni-Ti	Farkas and Roqueta (Ref. 17)

EAM potentials for these pure metals have been developed and tested to various levels in the past ten years since the original introduction of the EAM technique. The Ni-H interaction was actually one of the first interactions to be studied within the method² and will therefore be the natural starting point for the present work. In addition, compatible mixed interaction potentials will allow the study of H in alloys through simulations in the ternary Me1-Me2-H system, where Me1 and Me2 stand for the two constituents of the binary alloy. The study of H effects in intermetallics also requires the potentials for the alloy system (Me1-Me2 interaction), which are available for the cases we chose here. Table I shows the potentials that we used for the various pure metals and alloys considered.

This paper is organized as follows: first, we will describe the EAM potentials we used for the pure metals, the intermetallics, and the hydrogen; next, we will discuss the fitting procedure to obtain the H-metal interaction potentials; finally, we will show the results of the simulation of introducing H impurities in different binary alloys.

II. INTERATOMIC POTENTIALS FOR THE PURE COMPONENTS AND INTERMETALLICS

A. Pure components

EAM functions for monoatomic systems may be transformed to a normalized form in which the embedding function has null first derivative at the equilibrium electron density. If this is the case, V is defined as an effective pair-interaction potential⁵ which controls the energy change of a block of atoms when the electron density at the atoms site is not significantly altered. We note that, with this transformation, EAM models which appear to be rather different are found to be quite similar.

For consistency, we decided to use all the monoatomic EAM functions in the effective pair approach. The transformation used is as follows:

$$F^{\text{eff}}(\rho) = F(\rho) - \rho F'(\rho_0), \quad (3)$$

$$V^{\text{eff}}(R) = V(r) + 2\rho(R)F'(\rho_0), \quad (4)$$

where ρ_0 is the electronic density in the perfect lattice of the pure metal.

The EAM potentials used for the pure metals are summarized in Table I. For fcc Ni, we used the interatomic potential

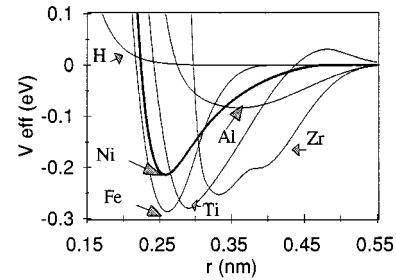


FIG. 1. Effective pair potentials for pure metals and H used in this work.

given by Voter and Chen.⁶ The potential was not originally in the effective pair scheme so we transformed it, keeping the electron density of the perfect lattice of Ni to 0.38 \AA^{-3} as given by Voter and co-workers. For fcc Al, we also used the functions given by Voter and Chen,⁶ transformed them to the effective pair approach and kept the electron density to 0.34 \AA^{-3} as stated in their work.

Embedded atom method interatomic potentials for hexagonal metals have been discussed by Oh and Johnson,⁷ Igarashi, Khantha, and Vitek,⁸ and more recently by Pasianot and Savino.⁹ The latter authors showed that there are two restrictive relations among the elastic constants for the method to be applicable using realistic embedding functions (F'' positive). These conditions are

$$(3C_{12} - C_{11})/2 > C_{13} - C_{44} > 0. \quad (5)$$

Experimental elastic constants for hcp Ti do satisfy these conditions. Pasianot and Savino also showed that the contribution of the so-called inner elastic constants in the hexagonal close packed lattice is important, and have taken this fact into account. Their potentials also have the embedding function adjusted so that the total cohesive energy fits the Rose *et al.* equation of state.¹⁰ We used these functions for Ti (already stated as effective-pair potentials) with the perfect lattice electron density normalized to 0.34 \AA^{-3} .

Elastic constants for hcp Zr do not comply with the restrictions imposed by Eq. (5). At most, Zr is a doubtful case depending on the number of neighbor shells included within the range of ϕ .⁹ Bearing these limitations in mind, we used the Zr potentials developed by Igarashi, Khantha, and Vitek⁸ after transforming them to effective pairs and normalizing the electronic density to 0.34 \AA^{-3} .

As for bcc Fe, we used the effective potentials developed by Simonelli, Pasianot, and Savino¹¹ normalizing the electronic density to 0.34 \AA^{-3} .

Finally, for H, we used the Baskes and Daw's 1984 parameterization of the first-principles calculations of Puska, Nieminen, and Manninen¹² after a transformation that will be described in the next section.

The effective pair potentials of all the pure components considered are shown in Fig. 1 and in the Appendix. In the course of the fitting procedure of the H-Me interactions, it was found that in order to maintain compatibility, it was essential to have all the potentials for the various metals considered in an effective pair scheme with very similar values of the electron density for the perfect lattice. If this con-

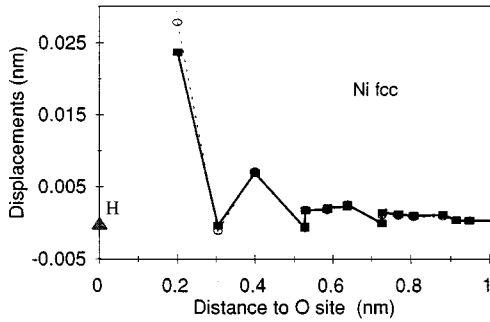


FIG. 2. Relaxation of the Ni lattice around the H impurity. The dashed curve corresponds to H EAM functions (Ref. 2), Ni (Ref. 6) and Ni-H interaction calculated with Eq. (6); solid curve to the same Ni EAM functions transformed to effective pairs, transformed H EAM potentials and Ni-H interaction from Table IV. Displacements practically coincide from the second-nearest neighbor on.

dition was not imposed, it was possible to develop one H-Me interaction but a second one using the same H functions could not be developed in general.

B. Intermetallics

As stated before, intermetallic potentials are needed to simulate ternary Me1-Me2-H systems. In this work, we present simulations of H impurities in alloys of the Ni-Al, Ti-Al, Ni-Ti, and Fe-Al systems; we used interatomic potentials for these systems that were developed previously (see Table I and the Appendix).

Embedded-atom simulations for various defects in Ni-Al have been carried out for several years now. There are several embedded-atom interatomic potentials developed for Ni-Al. The potentials developed by Voter and Chen⁶ and those developed at Sandia¹³ are based on the $L1_2$, Ni₃Al phase. Rao, Woodward, and Parthasarathy¹⁴ developed potentials based on $B2$ NiAl. In recent work,¹⁵ we derived mixed Ni-Al interaction potentials that are based on the $B2$ NiAl phase, while using the same Ni and Al potentials of Voter and Chen⁶ in an effective pair scheme. These latter potentials are used in the present work.

The Ti-Al case is more complicated since the embedded-atom method cannot properly model the elastic constants in these alloys due to the importance of angular-dependent forces in this system.¹⁴ We have recently developed Ti-Al interatomic potentials using the embedded atom and the related embedded defect technique,¹⁵ and derived interatomic potentials for the Ti-Al system with and without angular forces. We are using the latter in the present work.

A particular problem to be faced in the Ni-Ti system is that the $B2$ phase is not stable at low temperatures. The experimental values that are available for cohesive energies are high-temperature values. Sluiter *et al.*¹⁶ calculated the cohesive energies of various phases in the system, but they point out that the values they obtained for the $B2$ phase underestimate the actual cohesive energy. In previous work,¹⁷ we have approached the problem by developing two different potentials, one based on the high-temperature experimental cohesive energy and the other based on first-principle simulations. Best results were obtained with the

TABLE II. Ni-H EAM simulations using Ni EAM functions as in Ref. 6, H EAM functions as in Ref. 2, Ni-H interaction from Eq. (6). Enthalpy values referred to Ni fcc and to the hydrogen molecular bond strength of 2.4 eV per atom (Ref. 2).

Properties	Experimental	Calculated
V_H (\AA^3)	2.48 (Ref. 1)	2.27
ΔH_∞ (eV/at. H)	0.17 (Ref. 2)	0.18
Migration energy (eV)	0.41 (Ref. 2)	0.35
a_0 NiH (\AA)	3.71 (Ref. 2)	3.60
ΔH_f NiH (kJ/g at. H)	5.02 (Ref. 32)	5.98

one based on experimental data at high temperatures and so it was chosen here.

The Fe-Al interatomic potential was developed by Vailhé and Farkas based on the $B2$ FeAl phase.¹⁸

III. INTERATOMIC METAL-HYDROGEN POTENTIALS: FITTING PROCEDURE

A. The Ni-H system: derivation of the EAM functions for hydrogen

We started by studying the Ni-H system because this system has been studied since the introduction of the EAM technique. We first simulated the Ni-H system using the EAM functions for hydrogen that were given by Daw and Baskes in 1984² and the interatomic potential of Voter and Chen⁶ for Ni. Without any transformations, we developed mixed H-Ni pair interaction functions using a linear combination of these

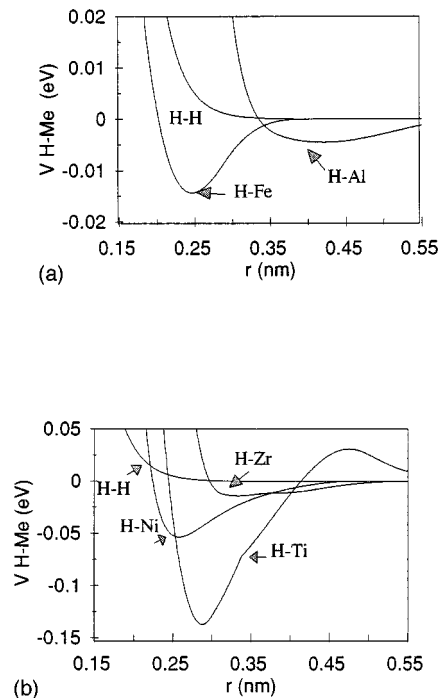


FIG. 3. Mixed Me-H interaction potentials, (a) with Me=Fe, Al, (b) Me=Zr, Ni, Ti.

TABLE III. Results for fcc H using the normalized transformed H potential.

Properties	This work	Calculated (Ref. 19)
Lattice parameter a_0 (nm)	0.265	0.228
Cohesive energy E_c (eV/at. H)	-1.803	-1.361

potentials for H and Ni. The functions were required to fit the heat of solution and the volume change upon the dissolution of hydrogen for this system. The best fit linear combination was obtained as follows:

$$V^{\text{Ni-H}}(r) = 0.25V^{\text{Ni-Ni}}(r) + 0.75V^{\text{H-H}}(r) \quad (6)$$

with $1.000 < r < 3.7895$. The V 's are in eV and r in Å.

The predicted relaxation of the Ni lattice around the H impurity using these potentials is shown in Fig. 2. The results of the simulation are listed in Table II.

The transformation of these functions to an effective pair scheme was investigated next, since this is important in developing compatibility with the interatomic potentials for the other metals. It is straightforward to transform the Ni functions given by Voter to effective potentials, as described previously. For hydrogen, the electronic density of a perfect metallic lattice is not known. Therefore, we chose to apply a transformation to the hydrogen potential such that the same linear combination of Eq. (6) will fit the experimental properties when both the H and the Ni are in effective pairs. The resulting transformation for hydrogen is the same as for effective pairs described in Eqs. (3) and (4), with $F'(\rho_0) = 15.00$. These functions will be referred to as the normalized EAM hydrogen functions.

The finally selected H-Ni interaction is shown in Fig. 3. The relaxation around the H impurity in Ni using these potentials is shown in Fig. 2, and is very similar to that of the case of the untransformed functions. Values of the energy of migration of H in Ni and the lattice parameter and the enthalpy of formation of the hydride are also coincident with those shown in Table II.

As an independent check, we used the set of normalized EAM functions for hydrogen to calculate the cohesive energy and lattice parameter of solid fcc hydrogen. The results are in Table III and they show good agreement with the first principles calculated values as reported in Ref. 19.

B. Fitting the metal-hydrogen interactions

The mixed metal-hydrogen pair interactions were then modeled by an empirical combination of the normalized

TABLE IV. Parameters obtained for the mixed Me-H interaction potential. Distances in 10^{-1} nm, calculated energies in eV.

Parameter	Ni-H	Al-H	Ti-H	Zr-H	Fe-H
A	0.250	0.045	0.600	0.055	0.050
a	1.0000	1.6000	1.0000	1.0000	0.8000
b	3.7895	4.5594	6.3118	8.0807	3.2000
c	1.0000	1.0000	0.8836	1.0000	0.9920
d	3.7895	4.5594	6.2953	8.0807	3.1034
e	1.0000	1.6000	1.0000	1.0000	0.9920
f	3.7895	4.5594	8.0870	8.0807	3.1034

EAM hydrogen functions and the effective potentials described above for the pure metals. The general form for all Me-H pair interactions is as follows:

$$V^{\text{Me-H}}(a+bx) = AV^{\text{Me-Me}}(c+dx) + (1-A)V^{\text{H-H}}(e+fx), \quad (7)$$

where x takes values from zero to unity; A and a through f are fitting parameters, most of them fixed by the potentials of the pure components. This formulation was chosen because of its generality while maintaining a basic functional form which is intermediate with those of the pure elements.

The parameters were obtained by a trial and error procedure fitting to the heat of solution at infinite dilution and predicting the volume of dissolution of hydrogen in metals. The parameters are shown in Table IV, the interatomic H-Me mixed potentials for Me=Ni, Al, Ti, Zr, Fe are reproduced in Fig. 3. Comparison of the experimental and fitted values can be seen in Tables V and VI, calculated lattice relaxations around the H impurity are seen in Table VII.

The heat of solution of H in a metal changes with the concentration of H. The experimental determination of the heat of solution at infinite dilution involves measurements of the enthalpy of dissolution at different H concentrations and extrapolation of the trend at low concentrations. Numerically, we determined the difference of energies of a block of metal atoms with one H atom in a defined interstitial position relative to the pure metal and the H_2 molecular bond strength of 2.4 eV atom.² As the size of the block of metal atoms increases (which is equivalent to reducing the H concentration of the system), so does the total energy of the system. At low H concentrations we are dealing with numerical errors in the heat of solution due to the difference of two large numbers. If the block of metal atoms is too small, however, we may have an ill-posed problem because of the border condi-

TABLE V. EAM simulations for pure metal-H systems. (O) means octahedral sites preferred.

Metal host	ΔH_∞ (eV/at. H)		V_H (Å ³)		B (eV/Å ³)	
	Calc.	Exp.	Calc.	Exp.	Eq. (10)	Pure host
Ni fcc	0.18 (O)	0.17 (Ref. 2)	2.38	2.48 (Ref. 1)	2.96	1.127
Al fcc	0.58 (O)	0.60 (Ref. 33)	3.97	...	5.40	0.494
Ti hcp	-0.48 (O)	-0.42 (Ref. 28)	2.41	2.78 (Ref. 1)	3.24	0.686
Zr hcp	-0.58 (O)	-0.52 (Ref. 28)	2.65	3.11 (Ref. 1)	6.95	0.607
Fe bcc	0.16 (O)	0.20 (Ref. 28)	3.16	2.9 (Ref. 1)	2.36	1.080

TABLE VI. EAM simulations for intermetallics. Enthalpy values referred to pure intermetallics and to the hydrogen molecular bond strength of 2.4 eV per atom (Ref. 2). (O) means octahedral sites preferred; (T) means tetrahedral sites preferred.

Metal host	ΔH_∞ (eV/at. H)	V_H (Å ³)		B (eV/Å ³)
	Calc.	Calc.	Eq. (10)	Pure host
Ni ₃ Al <i>L1</i> ₂	0.28 (O) Ni rich	4.87	3.41	0.913
NiAl <i>B2</i>	2.97 (T)	5.46	7.04	0.9
FeAl <i>B2</i>	2.82 (O) Al rich	5.49	4.07	0.9
NiTi <i>B2</i>	0.08 (T)	3.62	2.73	0.89
TiAl <i>L1</i> ₀	2.13 (O) Ti rich	4.86	4.69	0.734
Ti ₃ Al <i>D0</i> ₁₉	0.99 (T) Ti rich			0.48

tions. We dealt with the problem repeating the calculations for different block sizes and then extrapolating our values. The extrapolated values for the pure metals are shown in Table V.

Another way of changing the H concentration is by fixing the size of the block of metal atoms and increasing the amount of H atoms. If this is the case, the H-H interactions are taken into account. We did these calculations for the case of Ni and the results are shown in Figure 4.

Dissolving n atoms of H in a metal changes the volume V of the metal by

$$\Delta V = nV_H, \quad (8)$$

where V_H is the characteristic volume change per hydrogen atom.²⁰ Multiplying V_H by the Avogadro's number, we obtain the mean partial molar volume. If N is the number of metal atoms of the crystal with volume V and Ω is the mean atomic volume of the metal, then the relative volume change due to an atomic fraction $c = n/N$ is

$$\Delta V/V = c(V_H/\Omega). \quad (9)$$

Calculating the relative volume change as a function of the hydrogen concentration, we can obtain V_H from the slope at infinite dilution. Again, there is a compromise between the need of a large block of metal atoms compared to the amount of H required by the physics of the problem and the precision of the numerical determination of ΔV , which declines with larger values of V . In the experimental methods $\Delta V/V$ can be measured to accuracies ranging from 10^{-4} to 10^{-7} (Ref. 20) exceeding the accuracy with which the hydrogen concentration c can be determined. The solubility of H in metals is normally very low. This may introduce errors in the experimental values of V_H . Regardless of these difficulties, an empirical rule^{1,20,21} states a $V_H \cong 2.9 \text{ \AA}^3$ for all metals.

The actual displacements of the lattice atoms by the H can be seen as arising from the application of virtual forces (Kanzaki forces) to each lattice atom so that these forces cause the same displacements as the H atom does. The relative volume change, $\Delta V/V$, is related to the trace of the dipole tensor P_{ij} of the force distribution as follows:

$$\Delta V/V = c/(3B\Omega) \text{ Trace } P_{ij}, \quad (10)$$

TABLE VII. Atomic displacements (in nm) as a function of distance to the H atom for the preferred sites.

Metal host	Interest. site H	Interest.		First neigh.	Sec. neigh.	Third neigh.
		a_0 (nm)	c_0 (nm)			
Ni fcc	O	0.352		0.024	-0.0003	0.0069
Al fcc	O	0.404		0.052	-0.002	0.012
Ti hcp	O	0.295	0.4686	0.043	-0.0040	0.0050
Zr hcp	O	0.323	0.5148	0.026	0.004	0.012
Fe bcc	T	0.287		0.037	-0.006	0.001
Ni ₃ Al <i>L1</i> ₂	O	0.356		0.027 (Ni)	0.0069 (Ni)	-0.0010 (Ni)
				0.0015 (Al)	0.0016 (Al)	0.0020 (Al)
NiAl <i>B2</i>	T	0.288		0.050 (Ni)	-0.0045 (Ni)	0.010 (Ni)
				0.035 (Al)	0.001 (Al)	0.0025 (Al)
FeAl <i>B2</i>	O	0.291		0.043 (Fe)	-0.002 (Fe)	0.011 (Fe)
				0.033 (Al)	0.009 (Al)	0.0013 (Al)
NiTi <i>B2</i>	T	0.300		0.045 (Ni)	-0.010 (Ni)	0.0024 (Ni)
				0.062 (Ti)	-0.009 (Ti)	0.022 (Ti)
TiAl <i>L1</i> ₀	O	0.395	0.414	0.025 (Ti)	-0.0015 (Ti)	0.009 (Ti)
				0.040 (Al)	0.006 (Al)	0.0001 (Al)
Ti ₃ Al <i>D0</i> ₁₉	T	0.574	0.468	0.038 (Ti)	-0.0037 (Ti)	0.012 (Ti)
				0.037 (Al)	-0.0087 (Al)	-0.035 (Al)

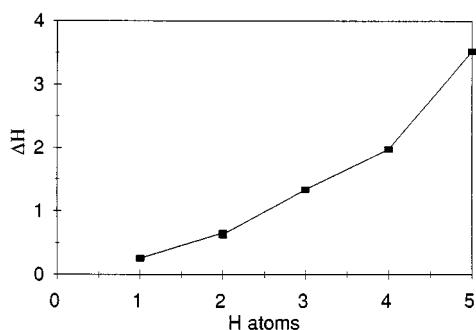


FIG. 4. H heat of solution (in eV) as a function of the number of H atoms placed at O sites in a block of 28 Ni atoms. The total number of Ni atoms is 256.

where B is the bulk modulus of the metal. In order to check consistency, we evaluated the trace of the dipole tensor and then calculated V_H from Eq. (10) with the values of B used to develop the pure metals EAM potentials (see Table V). The displacements of the H nearest neighbors are shown in Table VII. The data in Table V indicate that the simulated value changes may be significantly different from the elastic predictions of Eq. (10).

The migration energy of H in metals was not used in the fitting procedure. The predicted value for H migration in Ni was calculated as 0.35 eV and showed good agreement with the experimental 0.41 eV.

IV. H IN INTERMETALLICS

Our results for the behavior of hydrogen in the various intermetallics modeled by these potentials are included in Table VI, together with those obtained for the pure metals. For every intermetallic, different types of interstitial sites were tested, with different chemical environment for the H and the preferences were established. In the fcc based structures, we found octahedral sites to be preferred, whereas for bcc based structures, tetrahedral sites were either preferred or showed very similar energies to the octahedral sites. Figure 5 shows schematic pictures of the preferred interstitial sites for hydrogen in the various intermetallics studied. The intermetallics are generally composed of atoms of different sizes, and from a hard spheres simple argument, they are characterized by denser packing than the pure metals. It was expected that larger lattice expansions are required to fit the hydrogen into the interstitial sites. Indeed, our results show larger volume changes for the intermetallics than those for pure metals, significantly larger than the 2.9 \AA^3 rule of thumb.

A. Hydrogen in the Ni-Al system

We compared two different octahedral sites for H in a Ni_3Al $L1_2$ cell: site (a), where the H atom was surrounded by four Ni and two Al atoms and site (b), where only Ni atoms surround the H. Situation (b) was favored energetically, since the heat of solution was 0.28 eV while it was 2.0 eV for the other case. The lattice relaxation for the favored arrangement can be seen in Table VII. These results are rea-

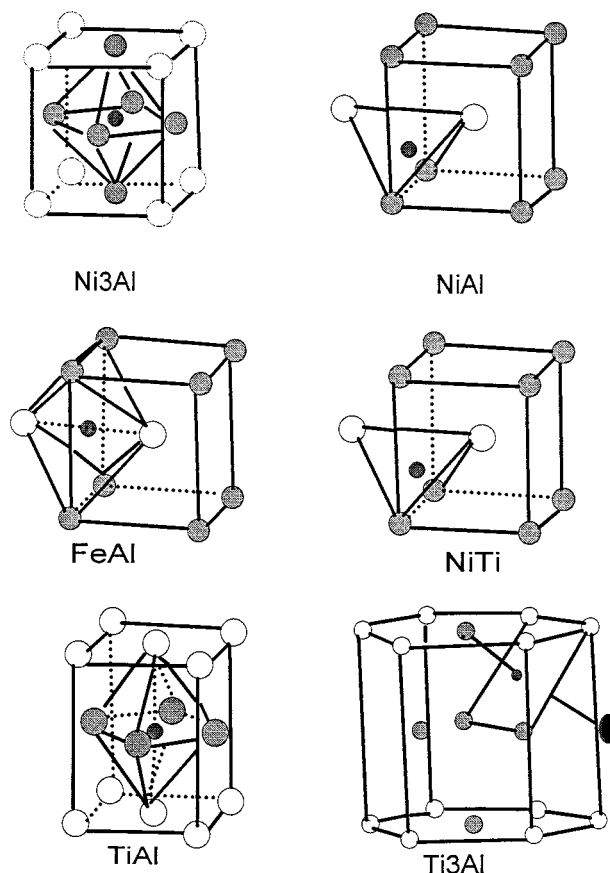


FIG. 5. Schematics of the preferred interstitial sites for hydrogen in the various intermetallics studied. Small filled circles correspond to H atoms; large open circles correspond to Al atoms whenever they are present; in NiTi, large open circles correspond to Ti atoms.

sonable since the H interaction with Al is the one that is energetically unfavorable. This means that H will prefer to segregate to sites that are characterized preferentially by a Ni-rich environment. This result should carry over to the case of grain boundary segregation where it may be expected that preferential segregation of H will be observed to Ni-rich grain boundaries as opposed to Al-rich boundaries. In general, for atomistic simulations,^{22,23} the weaker grain boundaries are those that are Al-rich boundaries and the stronger ones are the Ni-rich boundaries which will be preferentially embrittled by H.

For $B2$ NiAl, the heat of solution is much larger than for the Ni_3Al case. The tetrahedral site is preferred with two neighbors that are Ni and two that are Al. This site is characterized by $\Delta H_\infty = 2.97$ eV. The octahedral site with four Al neighbors and two Ni neighbors was the next preferred site with $\Delta H_\infty = 3.04$ eV. At first, it is surprising that this site is preferred to the octahedral site with four Ni neighbors and two Al neighbors, since the affinity of H for Ni is stronger than that for Al. The reason for this preference lies in the fact that in the bcc lattice, the octahedral sites are not regular and the preferred site is such that the shortest distances are from the hydrogen to the Ni, whereas the longer distances are

between the hydrogen and the Al. The hydrogen in the tetrahedral (preferred site) relaxed, so as to increase its distances to Al and decrease its distance to the Ni neighbors.

B. Hydrogen in the Ti-Al system

We compared the heats of solution of H in tetragonal TiAl putting the H in two different octahedral sites. Both situations were endothermic and the site where the H was surrounded by more Ti atoms was energetically preferred. Results of the preferred arrangement are shown in Tables V and VI. The energy per hydrogen atom in the nonpreferred site was found to be 2.76 eV, significantly higher than the 2.13 eV found for the preferred site.

The Ti_3Al intermetallic has an hcp-based structure with $c/a < 1$. Again, the preferred site for the hydrogen was with more neighboring Ti atoms and less Al. This is in agreement with the results of Gupta and Rodriguez for *ab initio* calculations performed on the Ti_3AlH hydride;²⁴ they conclude that the Ti-H interaction dominates the hydrogen bonding properties in this system. The heat of solution was less endothermic than for the $L1_0$ TiAl.

The preferred site was a tetrahedral site, with $\Delta H_\infty = 0.99$ eV. The next energetically favorable site had an energy $\Delta H_\infty = 1.13$ eV.

C. Hydrogen in FeAl

In FeAl, the preferred site is an octahedral with two Fe neighbors at the shortest distances and four Al neighbors at the longer distances ($\Delta H_\infty = 2.82$ eV). This is similar to the result obtained for octahedral sites in NiAl. In FeAl, the tetrahedral site was found to have an energy only slightly higher than the octahedral (2.85 eV). In this site, it was found that the H is displaced from the center of the site during relaxation so as to have longer distances with the Al neighbors (2.29 Å) and shorter distances with the Fe neighbors (1.90 Å).

The calculation showed no particular differences between placing the H in the O or T sites. The O site was slightly favored energetically, but within the error of the method. We found the H moved so that the distance between the Fe-H was shorter than the distance between Al-H in the relaxed configuration.

D. Hydrogen in NiTi

We also studied H in $B2$ NiTi. Hydrogen is quite soluble in this intermetallic with a low $\Delta H_\infty = 0.08$ eV for the tetrahedral site. The next energetically favored site is the octahedral one with two Ni neighbors at the shortest distances and four Ti neighbors at the longer distances. In this case, this type of site is expected from both a size consideration (Ti is a larger atom) and an affinity consideration with Ti. Due to the shortest distances, H is found to interact mostly with Ni in spite of its greater affinity for Ti. The same situation was reported for the hydride of the TiNi intermetallic by Gupta and Rodriguez,²⁴ performing *ab initio* calculations on that system, and also by Soubeyrou *et al.*²⁵

V. DISCUSSION

Hydrogen in pure metals: The results of our simulations for H in Ni are similar to those of Baskes and co-workers.²⁶ This is not surprising since our potentials for H are derived for Baskes' adaptation of the first principle's calculations of Puska and Nieminen, for the case of H in Ni.

Aluminum dissolves hydrogen endothermically in very small amounts. Reference 27 gives a review of solubility data at 1 atm hydrogen pressure and calculates from them a heat of solution of hydrogen in solid aluminum of 0.60 eV/at. H. Using these data to adjust the Al-H interaction potential, we obtained a weak interaction, as can be seen in Fig. 2. Since this interaction Al-H is not strong, we expect the resulting potential to be adequate to deal with ternary systems Al-Me-H in spite of minor errors. No data on lattice expansion of solid Al fcc with hydrogen at dilute concentrations are available, except for muon-spin-rotation experiments referred to in Ref. 28, which estimate the relaxation of the first-nearest neighbors to be relatively large, about 5%. The value of V_H we obtained is larger but not far apart from the empiric rule of 2.9 Å.

Hydrogen dissolves exothermically in hcp αTi at relatively low hydrogen pressures and expands the metal lattice. With increasing H to metal ratios, a metastable fct hydride forms and then a stable fcc nonstoichiometric dihydride, with vacancies in the H interstitial sublattice. We modeled the H-Ti pair potential as a linear combination of both the H effective pair potential and the Pasianot and Savino Ti potential,⁹ and then fitted the parameters to the heat of solution and the V_H of Ti in order to reproduce the two lattice parameters of the hcp lattice.

The location of the atoms of the light interstitial elements in the α Ti phase is an unresolved problem. San Martin and Manchester²⁹ concluded that after analyzing experimental evidences favoring either O or T sites at temperatures above 433 K. We decided to do the fitting with the H in an O site ($\Delta H_\infty = -0.48$ eV) and then calculated the situation with the H in a T site. The resulting enthalpy of dissolution ($\Delta H_\infty = -0.43$ eV) showed a slight energetic advantage for the octahedral site.

Zr and Ti behave in a very similar way with respect to hydrogen at $P = 1$ atm (see the assessed Ti-H and Zr-H phase diagrams in Refs. 29 and 30). It seemed natural to model the Zr-H interaction as we did the Ti-H. However, as was stated above, the experimental elastic constants of pure Zr hcp do not comply with the restriction imposed by the EAM model for hcp structures, so we adjusted the Zr-H interaction to a simpler linear combination than the one used for Ti (see Table IV).

Fe bcc is a poor endothermic H absorber. There is evidence in the literature¹ that the tetrahedral interstitial sites are preferred to the octahedral ones in bcc lattices. The difference of the calculated enthalpies of dissolution of H at infinite dilution between the two sites was 6 meV and favored the O site; this value is within the error of the method ($\Delta H_\infty = 0.157$ eV for H in the O site, 0.163 eV for H in the T site). Our results coincide with Puska and Nieminen's,²⁸ obtained when applying the effective-medium theory. The calculated V_H is larger than the experimental one.

In general, we found that the behavior of H in the metals

studied is nonelastic, yielding no agreement of simulated volume expansions with those calculated based on elasticity [Eq. (10)]. The values of the volume expansion for intermetallics were found to be significantly higher than the 2.9 \AA^3 generally found for pure metals. We propose to interpret this result due to denser packing in the ordered intermetallic structures. In the aluminides with fcc based structures, there is a general preference for H to avoid bonds with the Al. In the bcc based structures NiAl and FeAl, the octahedral and tetrahedral sites have very similar energies, with a difference that is similar to the error involved in EAM-type simulations. The type of octahedral site preferred in these materials involves more Al neighbors, a fact that may be explained on the basis of size considerations, since this type of site presents larger distances to the Al atoms. In the tetrahedral sites, the hydrogen relaxes in order to increase its distance to the Al atoms. In NiTi, the tetrahedral site is preferred followed by the octahedral site with more Ti atoms. This site is favored because of both size considerations and chemical affinity, resulting in the low value for the heat of solutions characteristic of this intermetallic.

VI. CONCLUSIONS

We developed empirical EAM interatomic potentials for several metal-H systems that used the same H functions. The EAM potentials for the pure elements involved were transformed to effective pairs and normalized to similar values of electronic density. The H EAM functions were obtained

from the H potentials used in Ref. 2 through a simple transformation. The interatomic metal-H potentials were then modeled as linear combinations of the transformed Me and H potentials and fitted to the heat of solution of H in metals at infinite dilution (ΔH_∞) and to the characteristic volume change per hydrogen atom (V_H).

We used the interatomic potentials to simulate the behavior of several intermetallics when a H impurity was introduced in them. We do not have experimental data to validate these results, but

(1) calculations predict higher values of V_H than the empirical rule.

(2) ΔH_∞ values seem high, but the trends are compatible with the thermodynamics.

(3) From energy values and lattice displacements we can see that the H atom seems to interact primarily with: (a) Ni in Ni-Al systems; (b) Ti in Ti-Al systems; (c) Fe in Fe-Al; (d) Ni in Ni-Ti.

ACKNOWLEDGMENTS

Valuable discussions with Juana Gervasoni and her help in the preliminary Ni-H calculations are gratefully acknowledged. This work was supported by the Office of Naval Research, Division of Materials Science and the National Science Foundation, International Programs, NSF-CONICET. D. Farkas also acknowledges financial support from Fulbright.

APPENDIX

Effective pair potentials used in this work, fitted to $V(r) = \sum_k a_k (ra_k - r)^3 H(ra_k - r)$:

	Ni	Al	Fe	Ti	Zr
a_1	-0.0431	-0.001 84	-0.1483	0.063 38	-0.0324
a_2	0.0809	-0.900	1.6561	-0.2109	9.8611
a_3	-0.000 36	6.9131	-0.7067	0.3378	9.755
a_4	6.318	59.6285	0.8460	0.6033	-2.6295
a_5	47.3871	-590.1682	-0.9193	-1.825	0.2896
a_6	197.0654			40	
ra_1	4.75	5.50	4.00	6.10	5.50
ra_2	4.00	3.50	3.00	5.50	3.35
ra_3	3.50	2.80	2.50	4.50	2.90
ra_4	2.58	2.00	2.00	2.75	2.50
ra_5	2.00	1.60	1.50	1.50	1.50
ra_6	1.50			0.88	
range	1.000	1.150	0.992 041	0.883 52	0
	4.7895	5.5554	4.095 403	6.195 326	5.494

Normalized electron density functions used in this work, adjusted to $\phi(r) = \sum_k b_k (rb_k - r)^3 H(rb_k - r)$:

	Ni	Al	Fe	Ti	Zr
b_1	0.002 634	0.001 419	-0.005 51	-0.0198	0.005 659
b_2	-0.005 73	0.001 571	0.118 013	0.017 65	-0.030 08
b_3	0.076 24	0.090 790	0.427 554	-0.050 29	0.097 95
b_4	-0.026 18	-0.588 60	2.663 861	0.024 11	0.3912
b_5	—	—	19.146 85	4.42	
rb_1	4.75	5.50	3.70	6.10	8.00
rb_2	3.50	3.50	3.00	5.00	6.40
rb_3	2.58	2.58	2.00	4.00	4.60
rb_4	1.50	1.50	1.50	3.00	2.00
rb_5			1.00	1.50	
range	1.0000	1.0000	0.99 204	0.8835	0
	4.7805	5.5554	4.0954	6.1953	8.08

Intermetallic potentials used in this work, adjusted to $V(r) = \sum_k a_k (ra_k - r)^3 H(ra_k - r)$:

	Ni-Al	Ti-Al	Fe-Al	Ni-Ti
a_1	-0.089 43	-0.027 33	-0.012 66	-0.000 47
a_2	0.2923	-0.3243	-0.1126	-0.027 19
a_3	0.1467	1.671	0.3665	-0.022 17
a_4	5.134	5.132	2.7468	0.4430
a_5	21.97	-35.2	3.0207	1.01
a_6		-255.7	-109.912	-0.8145
a_7				1.041
ra_1	4.75	4.75	5.00	6.00
ra_2	4.00	4.00	3.80	4.75
ra_3	3.50	3.50	3.35	4.00
ra_4	2.58	2.58	2.658	3.50
ra_5	2.00	2.00	2.25	2.58
ra_6	1.50	1.50	1.50	2.00
ra_7				1.50
range	1.0036	1.367	1.1100	1.0000
	5.58	5.269	4.0980	6.0000

H-metallic potentials used in this work, adjusted to $V(r) = \sum_k a_k (ra_k - r)^3 H(ra_k - r)$:

	Ni-H	Fe-H	Al-H	Ti-H	Zr-H
a_1	0.011 07	-0.011 72	-0.010 89	0.002 56	-0.001 833 9
a_2	0.023 33	0.1361	0.070 40	-0.0639	0.5541
a_3	-0.008 739	-0.2597	-0.2295	0.3124	0.4610
a_4	0.027 00	1.033	2.644 117	0.2525	0.2093
a_5	12.10	71.94	8.969 892	-0.0927	4.4860
a_6	52.30		-45.4361	1.8683	
a_7				-2.6604	
ra_1	4.75	3.95	6.00	6.19	5.50
ra_2	4.00	3.00	5.00	4.72	3.35
ra_3	3.50	2.48	4.00	3.70	2.90
ra_4	2.58	2.00	3.00	2.80	2.50
ra_5	2.00	0.95	2.00	2.30	1.50
ra_6	1.50		1.55	1.45	
ra_7				1.10	
range	1.0000-4.7895	0.8000-4.0000	1.0000-4.7895	0.8835-6.1953	0.9588-

Effective embedding functions adjusted to $F(\rho) = a + b\sqrt{\rho} + c\rho$:

	Ni	Al	Fe	Ti	Zr
<i>a</i>	0.655 07	0.7461	-0.575 461 22	0.418 41	0
<i>b</i>	-10.3219	-10.4406	-7.122 742 9	-10.738 163	-15.41
<i>c</i>	7.444 286	7.874 589	6.418 342 9	9.796 648 9	13.21
range	0	0	0.033 98	0.034 156 2	0
	0.505	0.55	0.5459	3.359 89	1.2639

- ¹Y. Fukai, in *The Metal-Hydrogen System*, Springer Series in Materials Sciences Vol. 21, edited by U. Gonser *et al.* (Springer-Verlag, Berlin, 1993).
- ²M. Daw and M. Baskes, *Phys. Rev. B* **29**, 6443 (1984).
- ³M. Finnis and J. Sinclair, *Philos. Mag. A* **50**, 45 (1984).
- ⁴S. Myers and M. Baskes, *Rev. Mod. Phys.* **64**, 559 (1994).
- ⁵R. A. Johnson, in *Many Atom Interactions in Solids*, Springer Proceedings in Physics Vol. 48 (Springer-Verlag, Berlin, 1990), p. 85.
- ⁶A. Voter and S. Chen, in *Characterization of Defects in Materials*, edited by R. W. Siegel *et al.*, MRS Symposia Proceedings No. 82 (Materials Research Society, Pittsburgh, 1987), pp. 175–180.
- ⁷D. Oh and R. Johnson, *J. Mater. Res.* **3**, 471 (1988).
- ⁸M. Igarashi, M. Khantha, and V. Vitek, *Philos. Mag. B* **63**, 603 (1991).
- ⁹R. Pasianot and E. Savino, *Phys. Rev. B* **45**, 12 704 (1992).
- ¹⁰J. H. Rose, J. R. Smith, F. Guinea, and J. Ferrante, *Phys. Rev. B* **29**, 2963 (1984).
- ¹¹G. Simonelli, R. Pasianot, and E. Savino, in *Materials Theory and Modelling*, edited by J. Broughton *et al.*, MRS Symposia Proceedings No. 291 (Materials Research Society, Pittsburgh, 1993), p. 567.
- ¹²M. Puska, R. Nieminen, and M. Manninen, *Phys. Rev. B* **24**, 3037 (1981).
- ¹³S. M. Foiles and M. S. Daw, *J. Mater. Res.* **2**, 5 (1987).
- ¹⁴S. Rao, C. Woodward, and T. A. Parthasarathy, in *High Temperature Ordered Intermetallic Alloys IV*, edited by L. Johnson *et al.*, MRS Symposia Proceedings No. 213 (Materials Research Society, Pittsburgh, 1991), p. 125.
- ¹⁵D. Farkas, B. Mutasa, C. Vaill e, and K. Ternes, *Model. Simul. Mater. Sci. Eng.* **3**, 201 (1994).
- ¹⁶M. Sluiter, P. E. A. Turchi, F. J. Pinski, and G. M. Stocks, *Mater. Sci. Eng. A* **152**, 1 (1992).
- ¹⁷D. Farkas, D. Roqueta, A. Vilette, and K. Ternes, *Model. Simul. Mater. Sci. Eng.* **4**, 1 (1996).
- ¹⁸C. Vaill e and D. Farkas (unpublished).
- ¹⁹*Calculated Electronic Properties of Metals*, edited by V. Moruzzi, J. Janak, and A. Williams (Pergamon, New York, 1978).
- ²⁰H. Peisl, in *Hydrogen in Metals I-Basic Properties*, Topics in Applied Physics Vol. 28, edited by G. Alefeld and J. Volkl (Springer-Verlag, Berlin, 1978), pp. 53–74.
- ²¹D. Westlake, *J. Less-Common Met.* **90**, 251 (1983).
- ²²G. Petton and D. Farkas, *Scr. Metall. Mater.* **25**, 55 (1991).
- ²³B. Mutasa and D. Farkas, *Mater. Sci. Forum* **207–209**, 305 (1996).
- ²⁴M. Gupta and E. Rodriguez, *J. Alloys Compd.* **219**, 6 (1995).
- ²⁵J. L. Soubeyrou, D. Fruchart, G. Lorthiorr, P. Ochinn, and C. Collin, *J. Alloys Compd.* **196**, 127 (1993).
- ²⁶S. Foiles, M. Baskes, C. Melius, and M. Daw, *J. Less-Common Met.* **130**, 465 (1987).
- ²⁷*Metal Hydrides*, edited by W. Mueller and J. B. G. Libowitz (Academic, New York, 1968).
- ²⁸M. Puska and R. Nieminen, *Phys. Rev. B* **29**, 5382 (1984).
- ²⁹A. San-Martin and F. Manchester, in *Phase Diagrams of Binary Titanium Alloys*, edited by J. L. Murray (ASM International, Metals Park, OH, 1990), pp. 123–135.
- ³⁰E. Zuzek, J. Abriata, A. San-Martin, and F. Manchester, in *Bulletin of Alloy Phase Diagrams* (ASM International, Metals Park, OH, 1990), Vol. 11, pp. 385–395.
- ³¹D. Farkas, *Model. Simul. Mater. Sci. Eng.* **2**, 975 (1994).
- ³²A. Switendick, *J. Less-Common Met.* **130**, 249 (1987).
- ³³R. Griessen, *Phys. Rev. B* **38**, 3690 (1988).